



A Near-Infrared Perfect Absorber Assisted by Tungsten-Covered Ridges

Buzheng Wei^{1,2} · Shuisheng Jian^{1,2}

Received: 8 April 2018 / Accepted: 22 June 2018 / Published online: 6 July 2018
© Springer Science+Business Media, LLC, part of Springer Nature 2018

Abstract

A periodic tungsten-covered dielectric ridge on substrate assembly is proposed in this article to investigate the perfect absorption in the near-infrared regime. The localized dipolar resonance and the propagating surface plasmon mode significantly restrict the reflectance thus forming two discrete absorption peaks. In the process of discovering perfect absorption, the geometrical parameters such as the tungsten layer thickness, ridge depth and width, substrate spacer thickness and the lateral period are correspondingly numerically explored and a rather high absorption rate of 99.9% can be achieved. Furthermore, the absorption peak is sensitive to the ground substrate index which makes it a potential candidate for compactly integrated on chip sensing applications. The polarization direction of the incident light modulates the absorption to a wider bandwidth and the oblique incidence splits the propagating mode along with a rather weak Fano-type absorption peak. The research may pave way for transition metal integrated on chip absorption system.

Keywords Absorber · Tungsten · Metamaterial

Introduction

The electromagnetic responses of naturally existed metals or metal compounds show superior abilities [1–4] when they are integrated into an artificially characterized metastructure, especially for the transition group of metals [5, 6]. Named as metamaterial absorbers [7], the functional patterns on a dielectric substrate attract enormous attentions and increasing interests for their unprecedented capabilities in light absorbing compared to solely processed block metals. The potential application prospects range from photovoltaics and solar cells [8], thermal radiation and imaging [9] to materials detection [10] and so on [11]. This man made series of metamaterial absorbers efficiently fill up

the blanked working region from infrared to terahertz frequencies [12]. A dual band gold split-ring resonator (SRR) on spacer is experimentally fabricated to estimate the terahertz absorption in 2010 [13]. Meanwhile, the metamaterial absorber can achieve polarization insensitivity when the structure is symmetric on both lateral and vertical dimensions [14]. In addition, 2D thin film material family including graphene makes a path in designing high-performance dynamically tunable metamaterial absorbers. To name one, to insert graphene between dielectrics which one side is geometrically loaded with arrays of elliptic dielectric cylinders expands the absorption bandwidth coming from two working mechanisms [15]. Usually within this optical band, the structure scale is usually several orders smaller than the source wavelength, so at interfaces of dielectric and metal/graphene, surface plasmon wave (SPW) is typically induced.

Surface plasmon polaritons (SPPs), which is an electromagnetic wave that can be excited on a metal-dielectric interface and decays exponentially into both neighboring media, has received increasing interests in both theoretical and experimental investigations [16]. SPPs are considered as one of the promising candidates to control nano-scale optical phenomena in sub- or deep subwavelength scale. For compact integrated micro- or nanophotonics, plenty

✉ Buzheng Wei
14111010@bjtu.edu.cn; 10273057@bjtu.edu.cn

¹ Key Lab of All Optical Network, Advanced Telecommunication Network of EMC, School of Electronic Information and Engineering, Beijing Jiaotong University, Beijing, 100044, China

² Institute of Lightwave Technology, Beijing Jiaotong University, Beijing, 100044, China

types of SPP-based devices, for instance, the biochemical sensors [17], filters [18], and Mach-Zehnder interferometers [19], have been studied and experimentally demonstrated [20]. Besides, more interestingly, with the combination of fiber Bragg grating inside the core, the energy can be transferred to a SPP with high efficiency at telecommunications wavelengths [21]. Tungsten, also known as wolfram, has remarkable robustness for the fact that it has the highest melting and boiling point, which is rarely found in near-infrared metamaterial absorbers. Recently, a sample demonstration of tungsten cross absorber at mid-infrared regime is proposed [22]. The combination of multiple tungsten crosses exhibits broadband near-perfect absorption. In [23], they have proposed a layered tungsten-based absorber while the maximum absorption remains to be challenged.

In this paper, we propose a tungsten-covered ridges metamaterial absorber working at near-infrared region. To get a better view of the formation mechanism, we observe the field profile of the cross section of the ridges in one unit cell and explore the geometrical parameter influences to the absorption rate. To modulate the light polarization direction and the incident angle, we get a better view of absorption on the dependencies of incident light. The numerical calculation method finite-difference time-domain is used to investigate the spectral responses and vast simulations are carried out to find a better design. In the end, conclusions are drawn.

Simulation and Method

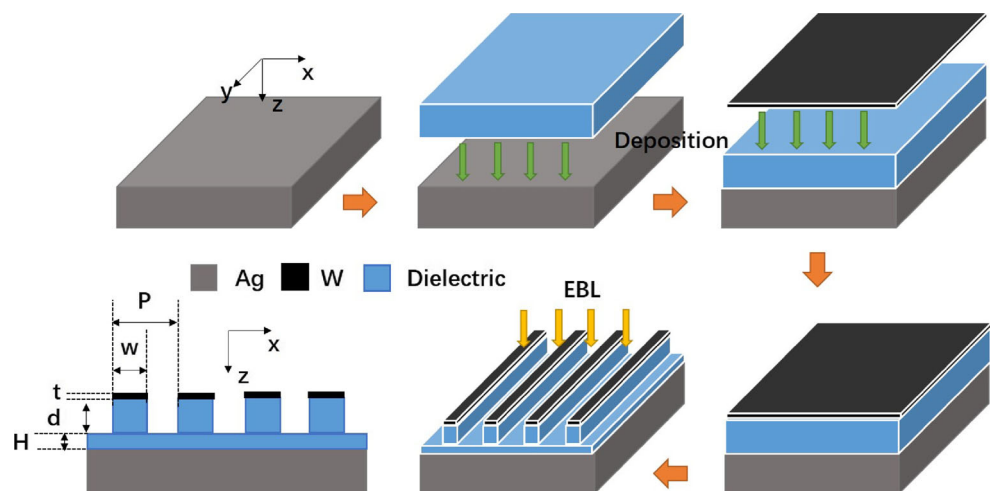
The periodic dielectric ridges covered by tungsten can be patterned using the electron beam lithography (EBL) after its deposition on the planar Ag mirror. The silver mirror is 500-nm thick to prevent the transmission and the skin depth is verified far less than 500 nm in the working wavelength

region [24]. The thickness of the dielectric spacer layer sandwiched between tungsten-covered ridges and silver is $H = 100$ nm while the etching depth is $d = 200$ nm. The top tungsten layer thickness is $t = 30$ nm. The lateral period is set to be $P = 800$ nm while the separation between the two adjacent ridges is 600 nm so the ridge width equals $w = 200$ nm. The schematic illustration of the tungsten absorber is dimensionally depicted in Fig. 1 alongside with the simplified production process. To get a better design of absorption, we carry out simulations using the finite-difference time-domain (FDTD) method in Lumerical commercial software FDTD 2016a. The dielectric constants of the tungsten and silver are all provided by the FDTD database from Palik book [25] while the refractive index of the dielectric spacer is $n = 1.45$. Since the device can be treated infinite long in y direction, a simplified 2D simulation model can be applied instead of the time and memory consuming 3D one. Periodic boundary conditions are used in x direction while perfectly matched layers (PMLs) are applied in z direction to absorb the reflected waves at the upper boundary. The mesh grid is set to be auto nonuniform at highest level 8. Besides, the light source is a transverse electric (TE) plane wave normally impinging on the device whose electric field polarization direction is parallel to x axis while the wave vector k_z points towards positive z axis according to the coordinate definition in Fig. 1. It is pointed out that the incident angle is the skewing from z axis, which we do not specially present it in Fig. 1.

Results and Discussions

Based on the settings in the above section, the absorption spectrum is numerically obtained by $A = 1 - R - T$, in which A , R , and T represent the absorption, reflectance, and transmission. As mentioned above, the transmission is

Fig. 1 The simplified production process and a schematic cross section view of the device. Structural parameters are labeled while the explanations are in text



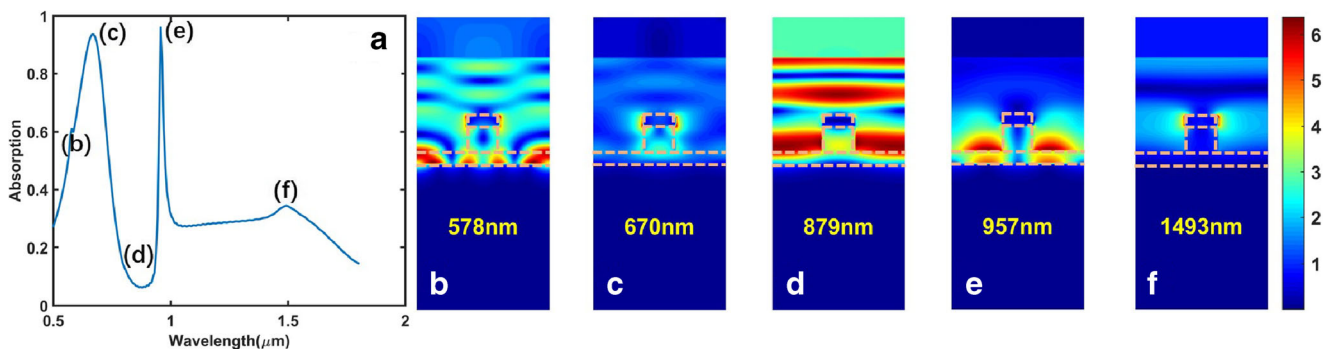


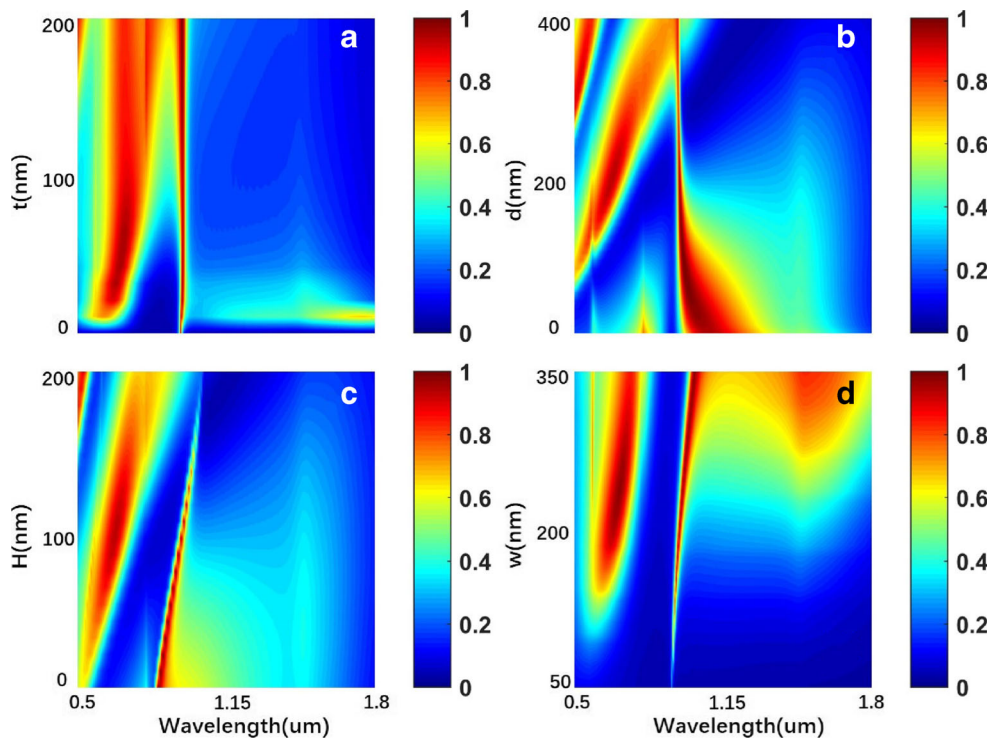
Fig. 2 **a** The absorption spectrum from 500 to 1800 nm. **b–f** The cross section electric field amplitude (V/m) distributions at several special wavelength points

eliminated due the thick silver mirror so the absorption is calculated as $A = 1 - R$. In Fig. 2a, two discrete resonant states are observed at 670 and 957 nm with quality factors (Q) 3.68 and 32.72, respectively. The low Q resonance state shows a relatively lower absorption rate of 93.7% while the high Q state absorption is 96.3%. One can note that the low Q resonant mode shows a relatively symmetric Lorentz line shape while the high Q mode shows rather asymmetric Fano line shape. The distinct line shapes of the two modes apparently reveal that the underlying physics of the formation is totally different. Thus, we plot the electric field distributions of five typical wavelength points labeled in Fig. 2a and elucidate them in Fig. 2b–f.

First of all, let us discuss the low Q mode resonance in Fig. 2c. When the light with resonant wavelength

travels to the tungsten-covered ridges, the localized electric dipole resonance mode is formed at the tungsten layer [26]. Under this condition, the periodic tungsten layers act as the nanoribbon resonators just like the graphene ribbon we investigate in Ref. [27]. Most energy is stored at both ends of the layer and the ridge substrate below resulting in a significant reduction in reflectance. Therefore, a distinct absorption peak is observed. Next, we move to the other high Q resonance mode absorption peak as shown in Fig. 2e. Much differently, no localized electric dipole mode is formed at the tungsten layer but a rather pronounced propagating surface plasmon mode is observed at dielectric-air and dielectric-silver interfaces. Though the confinement is several orders poorer than the low Q mode condition, the absorption is even higher. Under this

Fig. 3 The absorption spectra when investigating the geometrical parameters **a** t , **b** d , **c** H , **d** w . When one parameter changes, the others keep unchanged



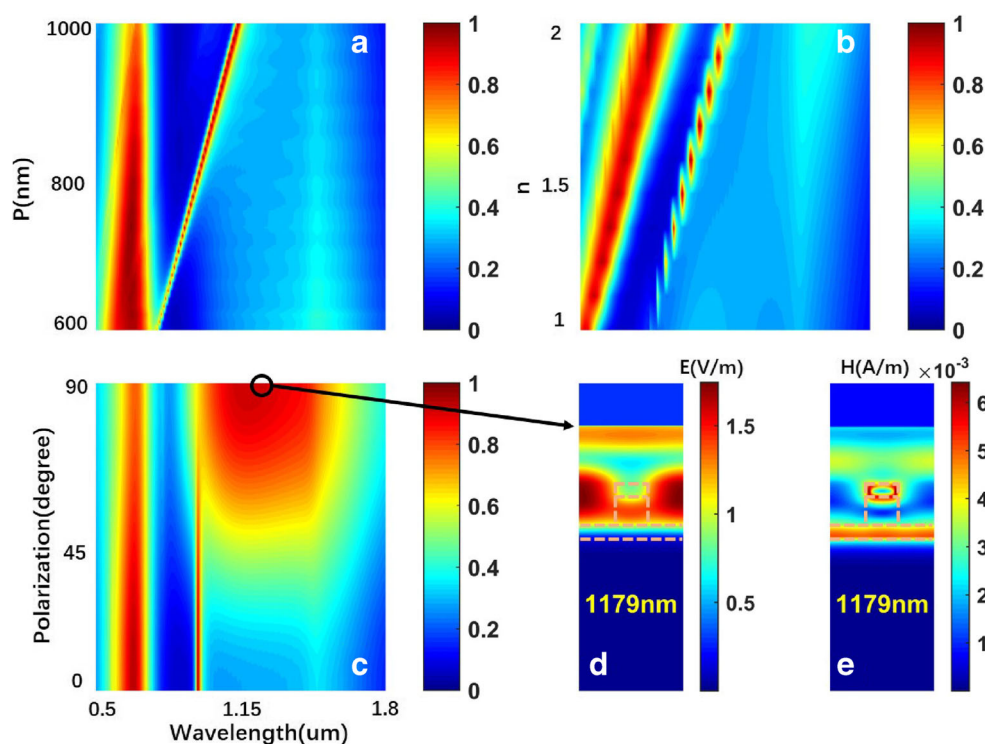
circumstance, the adjacently distributed ridges here act as the long period grating and when the wavelength satisfies the phase-matching condition [28], the propagating surface standing wave can be well created. It should be noted that in this condition, the period and the refractive index of the dielectric substrate must have an impact. At last, Fig. 2b represents the small tip at 578 nm, where the hybridized resonance of the aforementioned low Q and high Q modes are all observed. As for the dip in Fig. 2d, almost no energy is stored and most of them are reflected back. Different from Fig. 2c, the energy storage in Fig. 2f only induces the localized resonance at tungsten layer and no area in the ridge substrate is enlightened. So compared to Fig. 2c, the tip at 1493 nm shows a lower absorption rate.

Usually, the geometric shape influences the tunability of the device significantly both on the resonant wavelength and the absorption level. Hence, in order to have a better view to design the absorber to work in the target place, a large number of numerical simulations are necessary before the practical production. Directly associated dimensional parameters are ridge thickness t , etching depth d , dielectric substrate thickness H , and ridge width w . When investigating one parameter, the others keep unchanged as those initial settings in Section 2. First, the tungsten layer thickness t is increased from 0 to 200 nm. To see in Fig. 3a, the low Q mode has a slightly red shift with broader bandwidth and lower absorption rate while the high Q mode remains highest absorption around 957 nm. When t equals 190 nm, the absorption reaches 99.9%.

When the tungsten layer thickness is increased, the dipole mode resonance induced at both ends of the layer becomes weaker, which is believed to cause the lower absorption. Second, when increasing the etching depth d from 0 to 400 nm, the low Q mode resonance has an apparent red shift but the absorption gets lower. When the depth is larger 230 nm, higher order of mode appears at shorter wavelength region. Meanwhile, one can notice that when the depth becomes shallower, the high Q mode bandwidth becomes increasingly large and the resonance peak red shifts towards longer wavelength region. The increasing bandwidth lower the quality factor as well. Third, when increasing the dielectric substrate thickness H from 0 to 200 nm, both resonance modes red shift and the absorption rate becomes lower. Finally, when increasing the ridge width w from 50 to 350 nm, the resonance wavelength has the same red shifting property as increasing H . But when the width is small, only propagating mode with a low absorption rate is observed. Localized mode can not be induced due to the short ridge width compared to wavelength scale. But when the ridge is wide enough, the absorption in the longer wavelength region increases due to more localized energy storage which is monitored similar to Fig. 2f.

Other than the geometric parameters, we have mentioned that the grating period and the dielectric substrate index are also crucial in modulating the absorption spectrum. When the grating period increases from 600 to 1000 nm, the low Q mode resonance absorption rate decreases without any wavelength shifting. The high Q mode resonance

Fig. 4 The absorption spectra when varying only **a** the period P or **b** the refractive index n of the dielectric substrate. **c** The absorption spectra when the light source turns from TE mode to TM mode. **d, e** are the electric and magnetic field distributions when the light is TM polarized at 1179 nm



wavelength shows a positive linear dependency on the period P . Similarly, when the refractive index is increased from 1 to 2, both modes show positive linear dependencies. And when the refractive index equals 2, the highest absorption rate of the low Q mode reaches 99.3%. The refractive index change versus absorption peak wavelength change is 403 nm/RIU. When the incident light is polarized from TE mode to transverse magnetic (TM) mode, the absorption of high Q mode gradually turns into another broad band resonance mode with average absorption rate of over 91% in 140-nm wide wavelength range. From the electric field distributions, one can see that most energy is stored between two adjacently located ridges and the surface plasmon propagating wave has poor electric field confinement compared to 957 nm, as illustrated in Fig. 4d. As for the magnetic field in Fig. 4f, localized magnetic mode are induced around tungsten layer and the substrate stores energy as well. Nevertheless, the magnetic field amplitude is rather limited compared to the electric field. So the majority of the energy is between the ridges.

Besides, we have fixed the light source at perpendicular incident angle for all the above discussions. Next, we use the Broadband Fixed Angle Source Technique (BFAST) provided by FDTD to investigate oblique incidence. Since the simulation is hard to converge beyond 60° , we vary the incident angle from 0 to 60° for better simulation results. The numerical results are obtained and illustrated in Fig. 5a. First of all, an apparent splitting for the high Q mode is observed. As the incidence grows more oblique, the separation bandwidth between the two splitting peaks gets larger. Both peaks show relatively linear dependencies on the incident angle. We thus plot the electric field at incidence 15° for the two splitting peaks at 814 and 1147 nm (see Fig. 5b, c).

Both resonance peaks show asymmetrical field distributions. However, when taking a close look at the field distribution patterns, one can notice that at 1147-nm peak, the plasmonic mode is still confined at the dielectric-air

interface although the confinement is poorer compared to perpendicular incidence. But for the 814-nm peak, most energy is stored at the corner of the ridge especially apparent in the left separation. The wave pattern is no longer a steady standing plasmonic wave but a rather traveling-standing wave hybridization. This phenomenon proves that when the light encounters the sharp corners, there must exist a leakage of light into the air or a thermal loss into the substrate. Therefore, compared to 1147-nm peak, 814-nm peak absorption rate is much lower. Second, when the incident angle is beyond 40° , the low Q mode absorption is almost eliminated. As indicated by the damping limit [29] of metal scattering loss under oblique incidence, when the incident angle gets larger, edge mode resonance cannot be formed because most energy is scattered back into the air. The electric field is also plotted in Fig. 5d for 15° incidence at 683 nm and the localized resonance field pattern is comparable to Fig. 2c. It worth noticing in the absorption spectra that when the incidence begins to get oblique, a new resonance peak occurs which has an intersection with the splitting high Q mode resonance from the low Q area. We spot that resonance at 650 nm when incident angle is also 15° and plot the electric field in Fig. 5e. From the field pattern, one can see that higher order of high Q mode appears at the interfaces compared to b and c. This relatively low absorption peak is also the propagating surface resonance. Moreover, it appears right beside the low Q mode profile which makes the absorption a Fano-like line. The low Q continuum state interferes with the high order Q discrete mode state, which is rather analogous to the formation of Fano type [30]. It is believed when the geometry is then well adjusted, perfect Fano-type absorption remains to be discovered.

Conclusion

In conclusion, a perfect tungsten-covered dielectric grating absorber is proposed and numerically investigated to

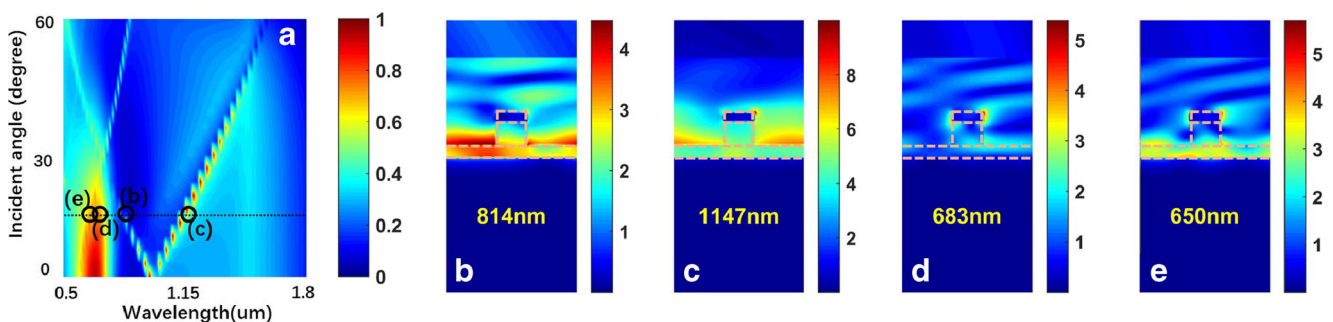


Fig. 5 a The absorption spectra when the incident light angle turns from 0 to 60° . **b–f** are the electric field amplitude (V/m) distributions at incident angle 15° at several typical points explained in the text, respectively

achieve a perfect absorption in the near-infrared region. The absorption is significantly enhanced due to the localized dipolar resonance at the edges of the tungsten layer and the surface propagating plasmon mode between the adjacent ridges. The dimensional parameters of the absorber play an important role in characterizing the absorption spectra while the absorption is also sensitive to the ground substrate index variations. When the light is TM polarized, a wide band absorption is achieved. Fano-type of absorption profile occurs when the incident light is obliquely launched. Overall, the design integrates the transition metal which may find potential use in on chip absorption system.

References

- Shelby R, Smith D, Schultz S (2001) Experimental verification of a negative index of refraction. *Science (New York, N.Y.)* 292(5514):77–79. <https://doi.org/10.1126/science.1058847>
- Smith DR, Padilla WJ, Vier DC, Nemat-Nasser SC, Schultz S (2000) Composite medium with simultaneously negative permeability and permittivity. *Phys Rev Lett* 84:4184–4187. <https://doi.org/10.1103/PhysRevLett.84.4184>, <https://link.aps.org/doi/10.1103/PhysRevLett.84.4184>
- Fang N, Lee H, Sun C, Zhang X (2005) Sub-diffraction-limited optical imaging with a silver superlens. *Science (New York, N.Y.)* 308(5721):534–537. <https://doi.org/10.1126/science.1108759>
- Song Z, Gao Z, Zhang Y, Zhang B (2014) Terahertz transparency of optically opaque metallic films. *EPL (Europhys Lett)* 106(2):27005. <http://stacks.iop.org/0295-5075/106/i=2/a=27005>
- Song Z, Wang K, Li J, Liu QH (2018) Broadband tunable terahertz absorber based on vanadium dioxide metamaterials. *Opt Express* 26(6):7148–7154. <https://doi.org/10.1364/OE.26.007148>. <http://www.opticsexpress.org/abstract.cfm?URI=oe-26-6-7148>
- Lei L, Li S, Huang H, Tao K, Xu P (2018) Ultra-broadband absorber from visible to near-infrared using plasmonic metamaterial. *Opt Express* 26(5):5686–5693. <https://doi.org/10.1364/oe.26.005686>
- Landy NI, Sajuyigbe S, Mock JJ, Smith DR, Padilla WJ (2008) Perfect metamaterial absorber. *Phys Rev Lett* 100:207402. <https://doi.org/10.1103/PhysRevLett.100.207402>. <https://link.aps.org/doi/10.1103/PhysRevLett.100.207402>
- Chagarov E, Sardashti K, Kummel AC, Lee YS, Haight R, Gershon TS (2016) Ag₂ZnSn(S,Se)₄: A highly promising absorber for thin film photovoltaics. *The Journal of Chemical Physics* 144(10):104704. <https://doi.org/10.1063/1.4943270>
- Schneider PC, France K, Gnther HM, Herczeg G, Robrade J, Bouvier J, McJunkin M, Schmitt JHMM (2015) X-ray to NIR emission from AA Tauri during the dim state - occultation of the inner disk and gas-to-dust ratio of the absorber*. *A&A* 584:A51. <https://doi.org/10.1051/0004-6361/201425583>
- Al-Bahi AM, Soliman AY, Mohamed NMA, Radioanal J (2018) Detection of illicit material using neutron activation: weakness and solutions. *Nucl Chem* 315(3):557–564. <https://doi.org/10.1007/s10967-017-5689-9>
- Wang BX, Wang GZ, Sang T, Wang LL (2017) Six-band terahertz metamaterial absorber based on the combination of multiple-order responses of metallic patches in a dual-layer stacked resonance structure. *Sci Rep* 7:41373. <https://doi.org/10.1038/srep41373>. <http://europemc.org/articles/PMC5264608>
- Tao H, Landy NI, Bingham CM, Zhang X, Averitt RD, Padilla WJ (2008) A metamaterial absorber for the terahertz regime: Design, fabrication and characterization. *Opt Express* 16(10):7181–7188. <https://doi.org/10.1364/OE.16.007181>. <http://www.opticsexpress.org/abstract.cfm?URI=oe-16-10-7181>
- Tao H, Bingham CM, Pilon D, Fan K, Strikwerda AC, Shrekenhamer D, Padilla WJ, Zhang RD, Averitt J (2010) A dual band terahertz metamaterial absorber. *J Phys D: Appl Phys* 43(22):225102. <http://stacks.iop.org/0022-3727/43/i=22/a=225102>
- Ma Y, Chen Q, Grant J, Saha SC, Khalid A, Cumming DRS (2011) A terahertz polarization insensitive dual band metamaterial absorber. *Opt Lett* 36(6):945–947. <http://ol.osa.org/abstract.cfm?URI=ol-36-6-945>
- Yang J, Zhu Z, Zhang J, Guo C, Xu W, Liu K, Yuan X, Qin S (2018) Broadband terahertz absorber based on multi-band continuous plasmon resonances in geometrically gradient dielectric-loaded graphene plasmon structure. *Sci Rep* 8(1):3239. <https://doi.org/10.1038/s41598-018-21705-2>. <http://europemc.org/articles/PMC5818652>
- Zayats AV, Smolyaninov II, Maradudin AA (2005) Nano-optics of surface plasmon polaritons. *Phys Rep* 408(3):131–314
- Apuzzo F, Limaj O, Di Gaspare A, Gilberti V, Domenici F, Sennato S, Bordi F, Lupi S, Ortolani M (2015) Mid-infrared Surface Plasmon Polariton Sensors Resonant with the Vibrational Modes of Phospholipid Layers. Springer, Netherlands, pp 439–441
- Fang Y, Hu J, Wang J (2013) Double-frequency filter based on coupling of cavity modes and surface plasmon polaritons. *IEEE Photonics J* 6(2):1–7
- Drezet A, Hohenau A, Stepanov AL, Dittlacher H, Steinberger B, Aussenegg FR, Leitner A, Krenn JR (2006) Surface plasmon polariton Mach-Zehnder interferometer and oscillation fringes. *Plasmonics* 1(2):141–145
- Okahisa S, Nakayama K, Nakayama Y, Ishii Y, Fukuda M (2016) Guiding properties of 1.31- and 1.55-um-wavelength surface plasmon polaritons on striped waveguides on silicon and their wavelength-selective detection. *J Lightwave Technol* 35(13):2702–2711
- Nemova G, Kashyap R (2006) Fiber-Bragg-grating-assisted surface plasmon-polariton sensor. *Opt Lett* 31(14):2118–2120
- Li Z, Stan L, Czaplowski DA, Yang X, Gao J (2018) Wavelength-selective mid-infrared metamaterial absorbers with multiple tungsten cross resonators. *Opt Express* 26(5):5616–5631. <https://doi.org/10.1364/OE.26.005616>. <http://www.opticsexpress.org/abstract.cfm?URI=oe-26-5-5616>
- Chirumamilla M, Roberts AS, Ding F, Wang D, Kristensen PK, Bozhevolnyi SI, Pedersen K (2016) Multilayer tungsten-alumina-based broadband light absorbers for high-temperature applications. *Opt Mater Express* 6(8):2704–2714. <https://doi.org/10.1364/OME.6.002704>. <http://www.osapublishing.org/ome/abstract.cfm?URI=ome-6-8-2704>
- Wang BX, Zhai X, Wang GZ, Huang WQ, Wang LL (2015) A novel dual-band terahertz metamaterial absorber for a sensor application. *J Appl Phys* 117(1):014504. <https://doi.org/10.1063/1.4905261>
- Palik E GG (1998) Handbook of optical constants of solids. Academic, New York
- Wang J, Tian H, Wang Y, Li X, Cao Y, Li L, Liu J, Zhou Z (2018) Liquid crystal terahertz modulator with plasmon-induced transparency metamaterial. *Opt Express* 26(5):5769–5776. <https://doi.org/10.1364/OE.26.005769>. <http://www.opticsexpress.org/abstract.cfm?URI=oe-26-5-5769>
- Buzheng Wei SJ (2017) Analog of midinfrared electromagnetically induced-transparency and slow rainbow trapping light based

- on graphene nanoribbon-coated silica substrate. *J. Nanophotonics* 11:11–11–9. <https://doi.org/10.1117/1.JNP.11.026011>
28. Wei B, Liu H, Ren G, Yang Y, Ye S, Pei L, Jian S (2017) Graphene based silicon–air grating structure to realize electromagnetically-induced-transparency and slow light effect. *Phys Lett A* 381(3): 160–165. <https://doi.org/10.1016/j.physleta.2016.10.034>. <http://www.sciencedirect.com/science/article/pii/S0375960116306703>
29. Liu N, Langguth L, Weiss T, Kästel J, Fleischhauer M, Fleischhauer T, Giessen H (2009) Plasmonic analogue of electromagnetically induced transparency at the drude damping limit. *Nat Mater* 8(9):758–762. <https://doi.org/10.1038/nmat2495>
30. Wei B, Jian S (2018) A nanoscale fano resonator by graphene-gold dipolar interference. *Plasmonics*. <https://doi.org/10.1007/s11468-018-0703-9>